Physico-Chemical Characterization of Anodic Oxides on Hf as a Function of the Anodizing Conditions

*Andrea Zaffora, Giada Tranchida, Francesco Di Franco, Francesco Di Quarto, Monica Santamaria**

Journal of The Electrochemical Society 163 (9) (2016) C563-C570

DOI: 10.1149/2.0871609jes

Electrochemical Materials Science Laboratory, DICAM, Università di Palermo, Viale delle Scienze, Ed. 6, Palermo, Italy

* Corresponding author

Abstract

Anodic films were grown to 5 V (Ag/AgCl) on mechanically polished Hf in 0.1 M ammonium biborate and 0.1 M NaOH. Independent of the anodizing conditions, the photoelectrochemical characterization allowed the observation of optical transitions at 3.25 eV, i.e. at photon energy lower than the band gap of HfO_2. They are attributed to localized states inside the gap of the oxide induced by the presence of oxygen vacancies. From the cathodic photocurrent spectra, it was possible to estimate an energy threshold of ~ 2.15 eV for internal electron photoemission phenomena. The impedance measurements proved the formation of insulating oxides with $\varepsilon = 19$. The anodizing occurs under a high field regime with an activation energy of 1.1 eV and an activation distance of 3.8 Å.

1 - Introduction

Within the past years, intense research has been carried out on HfO_2 as high dielectric constant material, a promising candidate to replace SiO_2 as gate dielectric in MOS based devices,[1–5] and as metal oxide for resistive random access memory (ReRAM).[6–8] For both technological applications, compact, uniform and flat oxides are necessary in order to reduce probability of oxide failure. Since hafnium is a valve metal, anodizing can be an efficient technique to prepare HfO_2 layers of controlled thickness, as recently proposed by Hassel and co-workers.[9,10]

Barrier type anodic films can be grown on valve metals such as Al, Ta, Nb, Ti, W, Zr, Hf, etc., by anodizing. i.e. an electrochemical process usually performed at room temperature, allowing for the growth of oxides with composition, thickness, morphology and properties easily tuneable by selecting the valve metals or valve metals alloy to be anodized, as well as the anodizing conditions (electrochemical bath, formation voltage).

The anodic films growth mechanism has been extensively studied in the past starting from earlier seminal work of 1961 by Young,[11] where the high field conduction model was proposed to describe the anodizing process. A deeper understanding of the ionic transport across the growing films was possible when experimental techniques based on radioactive tracers,[12] ion implantation[13] and nuclear analytic techniques[14] allowed following the cation and ionic fluxes sustaining the film growth during the anodizing process. Steps forward on the knowledge of all the species involved in the anodizing process, even those incorporated from the electrolyte, were made with the development of ultramicrotomy,[15] enabling the direct observation in transmission electron microscope of anodic films cross sections, and with Rutherford Back Scattering (RBS) and by Glow Discharge Optical Emission Spectroscopy (GDOES), making available compositional depth profiles of the anodic films.[16,17]

Anodizing of valve metals usually proceeds by simultaneous outwards migration of valve metal cations (oxidized at metal/oxide interface) and inwards migration of anions (namely O^{2-}/OH^-), developing film material both at the film/electrolyte and metal/film interfaces. Cations and anions

carry ionic current in a percentage directly proportional to their transport number. According to previous results reported in the literature, with exception of Zr and Hf, transport number of metal cations is comparable to the transport number of O^{2-}.[12] Ionic current during anodizing of Zr and Hf is almost entirely sustained by anions migration, less than 5 % being carried by metal cations.[12]

A survey of the already published works on Hf anodizing reveals that only a few papers have addressed the study of the kinetic of growth of anodic oxides,[18,19] reporting kinetic parameters far from each other. In this work we want to study the mechanism of growth of anodic films on Hf by anodizing the metal in ammonium biborate and sodium hydroxide aqueous solutions. Anodizing is performed under potentiodynamic conditions at several constant potential scan rates to check if the dependence of the anodizing current density on the electric field strength across the growing oxide is well described by the high field mechanism. Electrochemical impedance measurements are also performed in order to get information on the electrical properties of the anodic films and on the dielectric constant as a function of the growing conditions. The investigation is also supported by photoelectrochemical measurements allowing to get information on the energetic of the metal/oxide/electrolyte interface and the presence of defects on the oxides that can induce the presence of allowed localized states inside the mobility gap of HfO_2, that can induce oxide instability and leakage current.

2- Experimental

Pure hafnium rod (0.5 cm diameter, 97% from Goodfellow Metal), embedded in a Teflon cylinder and sealed through a two components epoxy resin (Torr Seal Varian Ass.), was used as working electrode in all the experiments. Electrode surface was abraded with P800 and P1200 papers and then rinsed with distilled water. Anodizing was carried out potentiodynamically up to 5 V vs. Ag/AgCl (0.197 V SHE) at different potential scan rates: 2, 5, 10, 20, 50, 100, 200, 500 and 1000 mV s^{-1}. Three electrodes setup was used for all the oxides growth with a Dimensionally Stable

Anode (RuO_2 activated TiO_2, $Ti_{0.7}Ru_{0.3}O_2$) net as counter electrode and an Ag/AgCl electrode as reference electrode. Anodizing electrolytes were 0.1 M NaOH (pH = 13) and 0.1 M ammonium biborate (ABE, $(NH_4)_2B_4O_7 \cdot 4H_2O$, pH ~ 9) aqueous solutions.

The experimental set-up for photoelectrochemical investigations was described elsewhere.[20,21] A 450 W UV-Vis xenon lamp, joined with a monochromator, allows irradiation of the working electrode through a quartz window. A two-phase lock-in amplifier was used, coupled with a mechanical chopper (chopping frequency = 13 Hz) that enables the separation of photocurrent from the total current circulating in the cell. All the experiments were performed in air at room temperature in 0.1 M ABE.

Impedance and differential capacitance measurements were carried out in a 0.25 M Na_2HPO_4 (pH~ 9) using a Parstat 2263 (PAR), connected to a computer for the data acquisition. A platinum net with a very high specific surface area was used as counter electrode, while Ag/AgCl electrode was used as reference electrode. Differential capacitance measurements were recorded by sweeping electrode potential from 3 to -0.8 V vs. Ag/AgCl with a constant a.c. frequency signal. The impedance spectra were generated by superimposing onto the continuous potential a sinusoidal signal of amplitude 10 mV over the frequency range 100 kHz–100 mHz, and the results were fitted using ZSimpWin software. Fitting parameters relating to measurements performed with at least three different anodic films grown in the same conditions (i.e. scan rate and anodizing solution) differ of less than 10%.

3- Results

3.1 - Anodizing behaviour

Mechanical polished Hf was anodized in 0.1 M ABE and 0.1 M NaOH potentiodynamically at several constant scan rates (ranging from 2 mV s^{-1} to 1 V s^{-1}). In Figures 1a and 1b we show the potentiodynamic curves recorded at all the scan rates in both the electrolytes. During the forward

scan, current suddenly increases and reaches an almost constant plateaux value, while it decreases rapidly during the reverse scan as expected for valve metals.[22,23] However the current density during potentiodynamic anodizing in NaOH solution is higher than that measured in ABE.

Under high field regime electric field strength, E_d, across a growing anodic oxide, and growth rate, dV/dt, are linked by the following equation:[11]

$$\frac{dV}{dt} = \eta \frac{jE_d M}{zF\rho} \frac{1}{r} \qquad [1]$$

where j is the measured current density, M is the molecular weight of the growing oxide (210.5 g mol^{-1}), z = 4 the number of electrons circulating per mole of formed oxide, F the Faraday constant, ρ the oxide density (9.68 g cm^{-3}), r the roughness factor (expressed as the ratio between the real and the geometrical surfaces) and η the growth efficiency. The latter accounts for the fraction of the overall circulating current, j_{tot}, dissipated in processes other than oxide formation, for instance oxygen evolution or oxide dissolution, thus:

$$\eta = \frac{j_{form}}{j_{tot}} \qquad [2]$$

where j_{form} is the current density effectively employed for the film formation. Eq 1 allows calculating for each scan rate the corresponding electric field strength, provided that r and η are known. We have estimated a roughness factor of ~ 1.2 comparing the growth curves relating to mechanical polished Hf and sputtering-deposited Hf, whose surface is flat at the nm scale. Concerning the growth efficiency, HfO_2 is reported to be chemically stable for pH > 4,[24] even if some authors report that hafnium oxides dissolves in strongly alkaline solutions.[25] If we assume η = 1, according to eq 1, E_d = 4.7 MV cm^{-1} and E_d = 4.3 MV cm^{-1} for anodizing Hf at 20 mV s^{-1} in 0.1

M ABE and 0.1 M NaOH, respectively. From the electric field strength it possible to estimate the anodizing ratio, A, i.e. the reciprocal of the electric field strength, providing an estimate of film thickening per each applied volt. Therefore, a thicker layer is expected to grow in NaOH.

3.2 – Photoelectrochemical measurements

Anodic photocurrent spectra (U_E = 3 V (Ag/AgCl)), relating to 5 V anodic films grown in both 0.1 M ABE and 0.1 M NaOH electrolytes at 10 mV s^{-1}, are reported in Figure 2a. The dependence of photocurrent on irradiating photon wavelength is not influenced by anodizing electrolyte. By assuming indirect optical transitions the following equation holds:[20,26]

$$\left(I_{ph}h\nu\right)^n \propto \left(h\nu - E_g^{opt}\right) \qquad [3]$$

in which I_{ph} is proportional to the light absorption coefficient and hν is the photon energy. According to eq 3, it is possible to estimate E_g^{opt} = 3.25 eV by extrapolating to zero the $(I_{ph}h\nu)^n$ vs. hν plot with n = 0.5 (shown in Figures 2b and 2c). This value is significantly lower than the band gap reported in the literature for HfO_2 (5.1 – 6.1 eV)[27–32] thus suggesting that the measured photocurrent is due to optical transitions involving allowed localized states inside the mobility gap of the oxide. Their origin, concentration and energy distributions have been extensively studied, due to the large interest on the electronic properties of hafnia in view of its possible application in MOS based devices.[1–5] They can be present even in a perfect crystal as a consequence of the potential well created in a perfect crystal by lattice polarization induced by the carriers themselves.[1] According to theoretical studies based on static approach and density functional theory, hole and electron polarons create localized states close to the valence and conduction band edges.[1,29] Localized states can be also generated by structural defects that, in the case of HfO_2, are mainly oxygen vacancies in different charge states. Oxygen vacancies in hafnia can be double or single

positively charged (V_o^{++}, V_o^{+}), neutral (V_o^{O}), and single or double negatively charged (V_o^{-}, V_o^{--}), depending on the number of trapped electrons.[29,30] On the basis of theoretical calculations of the formation energy of each defect, the dominant defect is expected to be V_o^{-}. The transition energy from the states generated by a significant concentration of single negatively charged oxygen vacancies to the conduction band is reported to be 3.2 eV by different authors.[29,30] This energy value is almost coincident with that estimated from Figure 2, thus suggesting the formation of an oxygen deficient hafnium oxide during the anodizing process in both solutions. It is important to mention that we are not able to determine the photocurrent due to optical transitions involving electrons from the valence band to the conduction band, since the experimental set up employed in this work has a very poor efficiency at short wavelengths (200 - 230 nm) , thus being very difficult to reveal photocurrent at the corresponding photon energy.

Dependence of photocurrent on applied electrode potential, i.e. electric field strength across the anodic film, was also studied under constant irradiating energy. As shown in Figure 3, by scanning the electrode potential downward at 10 mV s^{-1}, photocurrent changes from anodic to cathodic, as suggested by the photocurrent phase angle (not reported) and as expected for an insulating oxide, where the photocurrent sign depends on the direction of the imposed electric field strength. i.e. on the potential with respect to the flat band potential, U_{FB}. Therefore, the zero photocurrent potential provides a rough estimated of the flat band potential of the oxide. In wide band gap oxides the inversion potential is usually higher than the flat band potential due to the occurrence of recombination phenomena involving photo-generated electron-hole pairs at low band bending.[33–35]

We have also recorded photocurrent spectra at a potential below the U_{FB}, as shown in Figure 4, where we report the I_{ph} vs. wavelength curves, recorded at U_E = - 1 V (Ag/AgCl) for oxides grown in both 0.1 M ABE and 0.1 M NaOH. At this low potential, a photocurrent tail appears in the long wavelength region of the spectra, as shown in Figure 4b (UV filter was used to avoid photocurrent doubling effects). As already found for other valve metal oxides and also reported for anodic films

on sputtering-deposited Hf, such photocurrent can be attributed to photoemission phenomena, involving electrons of the metallic hafnium promoted to the conduction band of the oxide. In such case the dependence of I_{ph} on photon energy is described by the Fowler law:[20,21,36]

$$\left(I_{ph}\right)^{0.5} \propto \left(h\nu - E_{th}\right) \qquad [4]$$

in which E_{th} is the energy distance between metal Fermi level, E_F^M, and oxide conduction band edge and can be estimated by extrapolating to zero the $(I_{ph})^{0.5}$ vs. hν plot (as shown in Figures 4c and 4d). E_{th} resulted to be ~ 2.15 ± 0.1 eV, independently on anodizing solution, in agreement with previous experimental results.[37]

In previous works we have shown that during the anodizing of other valve metals in ammonium ion containing solutions, such as ABE, N incorporation occurs provided that the pH of the anodizing bath is higher than the pH of zero charge of the oxides[35,38–40]. N incorporation induces the formation of allowed localized states close to the valence band edges of the anodic oxides. Even though the pH of zero charge of HfO_2 is lower than 9 (pH_{pzc} =7.1),[41] the anodic films grown in ABE have the same photoelectrochemical behaviour of anodic films grown in 0.1 M NaOH. Therefore, we conclude that N incorporation does not occur appreciably in the case of Hf and/or the corresponding localized states are very close to valence band edge and do not induce any change in the photoelectrochemical behaviour of the oxide.

The same photoelectrochemical characterization has been performed for anodic films grown on Hf at different scan rates. In Table 1 we summarized the results obtained for films formed in 0.1 M ABE, confirming that the photoelectrochemical behaviour is almost independent of the growth rate.

3.3 - Impedance measurements

In Figures 5a and 5b we report electrochemical impedance spectra in the Bode representation (i.e. impedance modulus and phase angle vs frequency, respectively), relating to anodic oxides grown on Hf in both 0.1 M ABE and 0.1 M NaOH electrolytes, recorded at U_E = 3 V (Ag/AgCl), i.e. under potential higher than the flat band potential. The impedance spectra can be very well simulated by the electrical circuit shown in Figure 5c, consisting of R_{el}, accounting for the electrolyte resistance, in series with a parallel between R_{ox}, representative of the oxides resistance, and Q_{ox} a Constant Phase Element (CPE) introduced to model oxide capacitance. Fitting parameters are reported in Table 2. The very high R_{ox} values as well as the CPE exponent n close to 1 suggest that anodic oxides behave almost like pure capacitors, as already reported for anodic films grown on valve metals.[23,34] It is worth mentioning that R_{ox} for the film grown in ABE is slightly higher than that estimated for the anodic oxide grown in NaOH, thus suggesting the formation of a less defective oxide at pH = 9. We have also recorded EIS spectra at potential lower than U_{FB} (see Figures 6a and 6b) and, notably, they were very similar to the high potential EIS spectra, as also confirmed by the fitting parameters reported in Table 2. The EIS spectra recorded for anodic oxides grown at different scan rates are very similar to those reported in Figures 5 and 6, thus suggesting the impedance of the film is not significantly influenced by the growth rate in agreement with the photoelectrochemical findings. This is confirmed by the fitting parameters of the EIS spectra under anodic polarization (U_E = 3 V (Ag/AgCl)) and cathodic polarization (U_E = -1 V (Ag/AgCl)) reported in Tables 3a and 3b.

In Figure 7 differential measured capacitance curves, recorded by sweeping electrode potential from 3 to - 0.8 V (Ag/AgCl), are reported. For films grown in both 0.1 M ABE and 0.1 M NaOH at all constant a.c. signal frequencies (i.e. 10 kHz, 1 kHz and 100 Hz), capacitance is almost independent of electrode potential and slightly dependent on frequency, as expected for defective insulating oxides.[23] However, the measured capacitance was slightly different, with a higher value measured for the film formed in alkaline solution. Assuming that the oxide can be modelled as a simple parallel plate capacitor, the oxide capacitance can expressed as:[42]

$$C = \frac{\varepsilon \varepsilon_0 r}{d} \qquad [5]$$

where ε_0 (8.85×10^{-14} F cm^{-1}) is the vacuum permittivity, ε the oxide dielectric constant and d its thickness. Assuming that dielectric constant of HfO_2 is 19,[9] it possible to estimate the oxide thickness from eq 5, once the measured capacitance has been corrected for the Helmholtz double layer capacitance (i.e. 20 μF cm^{-2}). We used the capacitance measured at 10 kHz to reduce the contribution to the capacitance arising from localized states inside the gap.[23,43] The film thicknesses estimated from the capacitance are reported in Table 4 and result do not differ significantly.

4 - Discussion

The experimental results reported in Section 3 allow insight into the mechanism of hafnium anodizing. The growth of anodic films on valve metals (of which Hf is an example) is presented as a problem of ionic conduction at high field strength, complicated by the occurrence of transfer processes at the metal/oxide and oxide/electrolyte interfaces.[11] The high field conduction has been studied in the case of the so called valve metals. The main assumption of the high field model is that anodic oxide growth is sustained by hopping of mobile ions acquiring energy from thermal agitation plus the applied electric field sufficient to jump the potential barrier and reach the next closest available site. Following Verwey,[44] the movement of ions within the film is the rate determining step for the overall growth process, while Mott and Cabrera[45,46] assumed as rate limiting step the entry of oxidized metal ions at the metal/film interface. Independent of the step controlling the overall growth process, according to the high field mechanism, an exponential dependence of the current density j on the electric field strength is expected, according to the following equation:[11]

$$j = N\nu q \exp\left(-\frac{W - \alpha a q E_d}{k_B T}\right) = j_0 \exp\left[\frac{\alpha a q (U_E - U_{FB})}{k_B T d}\right] \quad [6]$$

in which N is the surface density of mobile ions, ν their vibrational frequency, q the charge associated with mobile ions, W the activation energy, αa is the activation distance or half barrier distance, given by the product between transfer coefficient α and the jump distance a, U_E is the applied potential, k_B is the Boltzmann constant and T the absolute temperature. In Figure 8 we report the logarithm of the plateau current density (averaged from at least 3 runs) as a function of electric field strength derived by anodizing Hf in 0.1 M ABE and 0.1 M NaOH, corresponding to different employed scan rates and derived according to eq 1. A linear dependence of ln j on E_d supports the ability of the high field model in describing the anodizing of Hf. Electric field strength between ~ 3 and 5.8 MV cm^{-1} was estimated as a function of the growth rate, comparable with previous values reported in the literature.[11,47,48] From the linear fit of this plot, it is also possible to calculate the parameters describing the kinetic of growth of the anodic oxides, j_0 and αa. We assumed q = 2 × 1.6 × 10^{-19} C, since according to previous results reported in the literature,[12,49] anodic films growth for hafnium is almost entirely sustained by migration of O^{2-}, while Hf^{4+} ions are almost immobile with a transport number ≤ 0.05. From the slope of the best fitting line we estimated a half jump distance of 3.8 Å, while an activation energy of 1.1 eV was estimated from the intercept during the anodizing of Hf in 0.1 M ABE. A half jump distance of 3.3 Å and an activation energy of 1.0 eV were estimated in relation to Hf anodizing in 0.1 M NaOH. αa well compares to the activation distance reported by Young[11] and with hopping distances calculated theoretically,[50] while it is far from other values reported in literature (that are significantly lower than the value expected according to the lattice parameters of m-HfO_2, which is the more stable hafnia polymorph at room temperature).[18,19]

The estimated barrier height has been compared with other values reported in the literature, and it was in very good agreement with the value reported by Young,[11] as well as with the value

calculated theoretically by density functional theory.[50] Notably, in the latter work the authors have also calculated the energy barrier for oxygen vacancy hopping, which is strongly dependent on the direction of motion, ranging from 90.47 meV along the <001> direction to 2814.79 meV along the <010> direction. The value estimated according to Figure 8 falls in this energy range.

The estimated kinetic parameters were used to simulate the potentiodynamic curve for the anodizing of Hf at 20 mV s^{-1} in 0.1 M ABE following the procedure described in literature.[51,52] The oxide thickness has been estimated according to the following equation:[52]

$$d = d_0 + \frac{M}{\rho z F}\left[\int j_{form}\,dt\right] = d_0 + \frac{M}{\rho z F}\left[\int \eta\, j_{tot}\,dt\right] \qquad [7]$$

where d_o is the thickness of the air formed oxide. If η is assumed to be constant, the film thickness can be computed by an iterative spreadsheet solution of eqs 6 and 7. As shown in Figure 9a, there is a very good agreement between the experimental and the simulated curves assuming d_0 = 15 Å, η ~ 1 and U_{FB} = - 0.8 V (Ag/AgCl). Moreover, the oxide thickness estimated according to eq 7 is almost coincident with that estimated from the capacitance. When the anodizing is performed in NaOH according to the kinetic parameters derived from Figure 8, assumption of η ~ 1 does not provide a good agreement between the thickness estimated from the capacitance and that estimated according to eq 7. We have to consider η < 1 and use αa and W derived from the growth curves recorded in ABE, where anodizing occurs at 100% efficiency. An efficiency of ~ 91% allows improvement of the fitting of the j-V curve, as shown in Figure 9b. The thickness of the anodic oxide grown to 5 V (Ag/AgCl) in NaOH is very close to that estimated from the capacitance (see Table 4). To get more insight into the phenomena responsible of an efficiency < 1, we have measured the oxide capacitance during potentiostatic polarization at 3 V (Ag/AgCl) in NaOH. As shown in Figure 10, a current density of 0.3 μA cm^{-2} was measured during the 1st hour of polarization, but it became negligible for longer times. The capacitance (and consequently the oxide thickness) measured after

each step of potentiostatic polarization (see Figure 10) remains almost constant, thus suggesting that the current is employed for oxide repairing and/or for oxygen evolution reaction.

All the experimental findings can be used to sketch the energetic of the metal/oxide/electrolyte interface, as depicted in Figure 11. In order to position the energy levels of Hf anodic oxide, we need to know Hf work function (3.9 eV)[53] and we set the oxide Fermi level, E_F^{ox}, according to the following equation:[33]

$$E_F^{ox} = -|e|U_{FB} + |e|U_{ref} \qquad [8]$$

in which e is the electron charge and U_{ref} is the potential of the Ag/AgCl reference electrode with respect to the vacuum scale.[54] The charge transfer for the oxygen evolution reaction at oxide films is usually explained in terms of electron tunnelling.[55] After the early stages of the anodizing process when oxide with thickness is > 2 nm, direct tunnelling is not probable, while it is likely that tunnelling occurs through localized states. The latter are transient states produced as a consequence of the mobile ions responsible of oxide growth and/or states generated by the presence of defects (for instance oxygen vacancies). The more negative equilibrium potential for O_2 evolution reaction in alkaline solution (and, thus, the higher available overvoltage) can account for the presence of a larger electronic current dissipated during the oxide formation in NaOH with respect to ABE.

5 – Conclusions

Anodic films were grown to 5 V (Ag/AgCl) on mechanical polished Hf in 0.1 M ABE and 0.1 M NaOH potentiodynamically at different scan rates. The photoelectrochemical characterization revealed that band gap, flat band potential and Fowler threshold are not significantly influenced by the anodizing electrolyte as well as by the growth rate. Optical transitions from allowed localized state inside the band gap of the anodic oxides to the conductions band were indicated, and are

associated with the presence of oxygen vacancies in the films. The conduction band edge was located at -1.75 eV with respect to the vacuum, according to the Fowler threshold. The impedance measurement allowed the conclusion that the oxides behave as insulating materials, with dielectric constant of 19.

The dependence of the anodizing current on the growth rate was studied in the frame of the high field model. Anodizing in ABE proceeds at high efficiency with an activation energy of 1.1 eV and an activation distance of 3.8 Å, which are physically reasonable if compared with other results reported in the literature. The anodizing in alkaline solutions occurs at lower efficiency due to the presence of oxide dissolution phenomena and/or oxygen evolution reaction.

The experimental findings provided the energetics of the Hf/anodic HfO_2/electrolyte interface, which is crucial to evaluate any technological application of the oxide.

References

1. D. Muñoz Ramo, A. L. Shluger, J. L. Gavartin, and G. Bersuker, *Phys. Rev. Lett.*, **99**, 155504 (2007).

2. A. Paskaleva, M. Rommel, A. Hutzler, D. Spassov, and A. J. Bauer, *ACS Appl. Mater. Interfaces*, **7**, 17032–17043 (2015).

3. L. S. Salomone, J. Lipovetzky, S. H. Carbonetto, M. A. García Inza, E. G. Redin, F. Campabadal, and A. Faigón, *Thin Solid Films*, **600**, 36–42 (2016).

4. A. G. Khairnar, L. S. Patil, R. S. Salunke, and A. M. Mahajan, *Indian J. Phys.*, **89**, 1177–1181 (2015).

5. J. Robertson and R. M. Wallace, *Mater. Sci. Eng. R Reports*, **88**, 1–41 (2015).

6. A. Wedig, M. Luebben, D.-Y. Cho, M. Moors, K. Skaja, V. Rana, T. Hasegawa, K. K. Adepalli, B. Yildiz, R. Waser, and I. Valov, *Nat. Nanotechnol.*, **11**, 67–74 (2016).

7. M. Wang, C. Bi, L. Li, S. Long, Q. Liu, H. Lv, N. Lu, P. Sun, and M. Liu, *Nat. Commun.*, **5**, 4598 (2014).

8. C. La Torre, K. Fleck, S. Starschich, E. Linn, R. Waser, and S. Menzel, *Phys. Status Solidi*, **213**, 316–319 (2016).

9. A. I. Mardare, C. M. Siket, A. Gavrilovi -Wohlmuther, C. Kleber, S. Bauer, and A. W. Hassel, *J. Electrochem. Soc.*, **162**, E30–E36 (2015).

10. C. M. Siket, M. Bendova, C. C. Mardare, J. Hubalek, S. Bauer, A. W. Hassel, and A. I. Mardare, *Electrochim. Acta*, **178**, 344–352 (2015).

11. L. Young, *Anodic Oxide Films*, Academic Press, London, (1961).

12. J. A. Davies, B. Domeij, J. P. S. Pringle, and F. Brown, *J. Electrochem. Soc.*, **112**, 675–680 (1965).

13. F. Brown and W. D. Mackintosh, *J. Electrochem. Soc.*, **120**, 1096–1120 (1973).

14. G. Amsel and D. Samuel, *J. Phys. Chem. Solids*, **23**, 1707–1718 (1962).

15. R. C. Furneaux, G. E. Thompson, and G. C. Wood, *Corros. Sci.*, **18**, 853–881 (1978).

16. K. Shimizu, G. M. Brown, H. Habazaki, K. Kobayashi, P. Skeldon, G. E. Thompson, and G. C. Wood, *Surf. Interface Anal.*, **27**, 24–28 (1999).

17. K. Shimizu, G. M. Brown, H. Habazaki, K. Kobayashi, P. Skeldon, G. E. Thompson, and G. C. Wood, *Electrochim. Acta*, **44**, 2297–2306 (1999).

18. H. A. Abd El-Rahman and M. M. Abou-Romia, *J. Appl. Electrochem.*, **20**, 39–44 (1990).

19. S. A. Salih, A. A. Abdel Khalek, and G. A. El Mahdy, *Bull. Soc. Chim. Fr.*, **128**, 665–670 (1991).

20. F. Di Quarto, F. La Mantia, and M. Santamaria, in *Modern Aspects of Electrochemistry, No. 46: Progress in Corrosion Science and Engineering I*, S.-I. Pyun and J.-W. Lee, Editors, p. 231–316, Springer, New York (2009).

21. M. Santamaria, F. Di Quarto, and H. Habazaki, *Electrochim. Acta*, **53**, 2272–2280 (2008).

22. F. Di Franco, G. Zampardi, M. Santamaria, F. Di Quarto, and H. Habazaki, *J. Electrochem. Soc.*, **159**, C33–C39 (2012).

23. F. Di Franco, M. Santamaria, F. Di Quarto, F. La Mantia, A. I. de Sa, and C. M. Rangel, *ECS J. Solid State Sci. Technol.*, **2**, N205–N210 (2013).

24. M. Pourbaix, *Atlas of electrochemical equilibria in aqueous solutions*, Pergamon Press, Oxford, UK, (1966).

25. A. G. Gad-Allah, H. A. Abd El-Rahman, and M. M. Abou-Romia, *J. Appl. Electrochem.*, **18**, 532–537 (1988).

26. F. Di Franco, P. Bocchetta, C. Cali', M. Mosca, M. Santamaria, and F. Di Quarto, *J. Electrochem. Soc.*, **158**, H50–H54 (2011).

27. V. V. Afanas'ev, A. Stesmans, F. Chen, X. Shi, and S. A. Campbell, *Appl. Phys. Lett.*, **81**, 1053 (2002).

28. A. R. Newmark and U. Stimming, *Electrochim. Acta*, **34**, 47–55 (1989).

29. D. Muñoz Ramo, J. L. Gavartin, A. L. Shluger, and G. Bersuker, *Phys. Rev. B*, **75**, 205336 (2007).

30. E. Hildebrandt, J. Kurian, and L. Alff, *J. Appl. Phys.*, **112**, 114112 (2012).

31. V. A. Gritsenko, T. V. Perevalov, and D. R. Islamov, *Phys. Rep.*, **613**, 1–20 (2016).

32. C. Bartels, J. W. Schultze, U. Stimming, and M. A. Habib, *Electrochim. Acta*, **27**, 129–140 (1982).

33. M. Santamaria, F. Di Franco, F. Di Quarto, P. Skeldon, and G. E. Thompson, *J. Phys. Chem. C*, **117**, 4201–4210 (2013).

34. A. Zaffora, F. Di Franco, M. Santamaria, H. Habazaki, and F. Di Quarto, *Electrochim. Acta*, **180**, 666–678 (2015).

35. A. Zaffora, M. Santamaria, F. Di Franco, H. Habazaki, and F. Di Quarto, *Phys. Chem. Chem. Phys.*, **18**, 351–360 (2016).

36. M. Santamaria, F. Di Quarto, P. Skeldon, and G. E. Thompson, *J. Electrochem. Soc.*, **153**, B518–B526 (2006).

37. F. Di Quarto, M. Santamaria, P. Skeldon, and G. E. Thompson, *Electrochim. Acta*, **48**, 1143–1156 (2003).

38. F. Di Franco, M. Santamaria, F. Di Quarto, E. Tsuji, and H. Habazaki, *Electrochim. Acta*, **59**, 382–386 (2012).

39. S. Miraghaei, M. Santamaria, and F. Di Quarto, *Electrochim. Acta*, **134**, 150–158 (2014).

40. A. Zaffora, M. Santamaria, F. Di Franco, H. Habazaki, and F. Di Quarto, *Electrochim. Acta*, **201**, 333–339 (2016).

41. E. McCafferty, *Electrochim. Acta*, **55**, 1630–1637 (2010).

42. R. P. Feynman, R. B. Leighton, and M. Sands, *The Feynman Lectures on Physics, Vol. II*, California Institute of Technology, (1963).

43. F. La Mantia, M. Santamaria, F. Di Quarto, and H. Habazaki, *J. Electrochem. Soc.*, **157**, C258–C267 (2010).

44. E. J. W. Verwey, *Physica*, **2**, 1059–1063 (1935).

45. N. F. Mott, *Trans. Faraday Soc.*, **43**, 429–434 (1947).

46. N. Cabrera and N. F. Mott, *Reports Prog. Phys.*, **12**, 163–184 (1949).

47. M. Santamaria, F. Di Quarto, S. Zanna, and P. Marcus, *Electrochim. Acta*, **56**, 10533–10542 (2011).

48. H. A. Johansen, G. B. Adams, and P. Van Rysselberghe, *J. Electrochem. Soc.*, **104**, 339–346 (1957).

49. M. Fogazza, M. Santamaria, F. Di Quarto, S. J. Garcia-Vergara, I. Molchan, P. Skeldon, G. E. Thompson, and H. Habazaki, *Electrochim. Acta*, **54**, 1070–1075 (2009).

50. Z. Wang, H. Yu, and H. Su, *Sci. Rep.*, **3**, 3246 (2013).

51. H. Lee, F. Xu, C. S. Jeffcoate, and H. S. Isaacs, *Electrochem. Solid-State Lett.*, **4**, B31–B34 (2001).

52. C. J. Boxley, J. J. Watkins, and H. S. White, *Electrochem. Solid-State Lett.*, **6**, B38–B41 (2003).

53. D. R. Lide, Ed., *CRC Handbook of Chemistry and Physics, 90th Edition*, CRC Press/Taylor and Francis, Boca Raton, (2010).

54. R. Memming, *Semiconductor Electrochemistry*, J. Wiley-VCH, Weinheim, (2001).

55. C. Hammer, B. Walther, H. Karabulut, and M. M. Lohrengel, *J. Solid State Electrochem.*, **15**, 1885–1891 (2011).

Tables

Growth scan rate ($mV\ s^{-1}$)	E_g^{opt} (eV)	E_{th} (eV)
2	3.21	2.10
10	3.25	2.25
50	3.26	2.13
1000	3.19	2.25

Table 1. Optical transition (E_g^{opt}) and threshold energy (E_{th}) for Hf anodic films grown at different scan rate in 0.1 M ABE.

Anodizing electrolyte	Electrode potential (V vs. Ag/AgCl)	R_{el} ($\Omega\ cm^2$)	R_{ox} ($\Omega\ cm^2$)	Q_{ox} ($S\ s^n\ cm^{-2}$)	n
0.1 M NaOH	3	8	9.61×10^5	1.78×10^{-6}	0.982
	-1	8	3.86×10^6	1.93×10^{-6}	0.974
0.1 M ABE	3	8	2.07×10^6	1.73×10^{-6}	0.985
	-1	8	1.13×10^7	1.85×10^{-6}	0.977

Table 2. Fitting parameters relating to EIS spectra of 5 V Hf anodic oxides, grown in ABE and NaOH, using equivalent electric circuit of Figure 5c.

Growth scan rate ($mV\ s^{-1}$)	R_{el} ($\Omega\ cm^2$)	R_{ox} ($\Omega\ cm^2$)	Q_{ox} ($S\ s^n\ cm^{-2}$)	n
2	8	1.69×10^6	1.69×10^{-6}	0.986
5	8	1.01×10^6	1.77×10^{-6}	0.986
20	8	1.38×10^6	1.78×10^{-6}	0.984
50	8	1.36×10^6	1.85×10^{-6}	0.977
100	8	9.57×10^5	1.85×10^{-6}	0.984
200	8	1.37×10^6	2.20×10^{-6}	0.979
500	8	9.68×10^5	2.00×10^{-6}	0.983
1000	8	9.91×10^5	2.13×10^{-6}	0.980

Table 3a. Fitting parameters relating to EIS spectra, recorded at 3 V vs. Ag/AgCl, of 5 V Hf anodic oxides, grown in ABE at different scan rates, using equivalent electric circuit of Figure 5c.

Growth scan rate ($mV\ s^{-1}$)	R_{el} ($\Omega\ cm^2$)	R_{ox} ($\Omega\ cm^2$)	Q_{ox} ($S\ s^n\ cm^{-2}$)	n
2	8	1.99×10^6	1.83×10^{-6}	0.977
5	8	4.13×10^6	1.90×10^{-6}	0.978
20	8	1.75×10^6	1.90×10^{-6}	0.976
50	8	2.59×10^6	1.98×10^{-6}	0.970
100	8	6.63×10^5	1.92×10^{-6}	0.981
200	8	1.35×10^5	2.22×10^{-6}	0.980
500	8	6.63×10^6	2.14×10^{-6}	0.975
1000	8	1.28×10^6	2.38×10^{-6}	0.968

Table 3b. Fitting parameters relating to EIS spectra, recorded at -1 V vs. Ag/AgCl, of 5 V Hf anodic oxides, grown in ABE at different scan rates, using equivalent electric circuit of Figure 5c.

Anodizing electrolyte	$d_{ox,Cap}$ (nm)	$d_{ox,Sim}$ (nm)
0.1 M NaOH	12.5	12.6
0.1 M ABE	12.9	12.4

Table 4. Oxide thicknesses calculated according eqs 5 and 7.

Figures

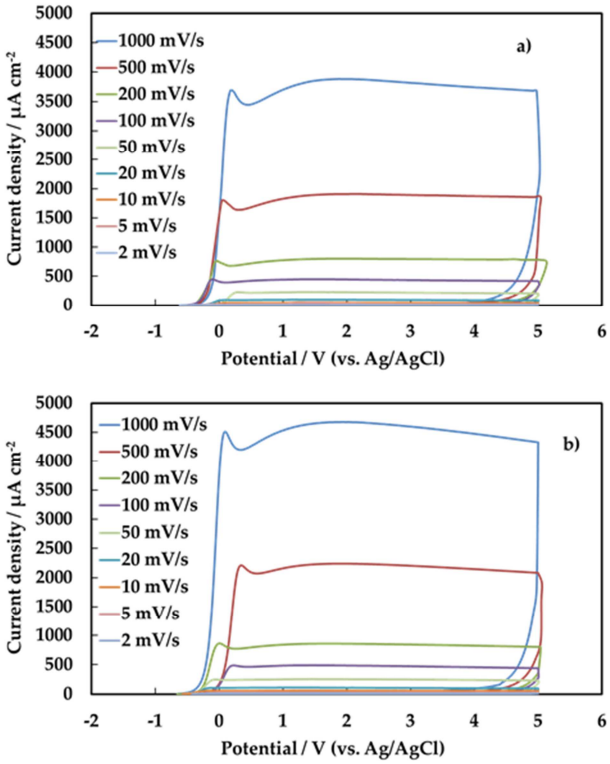

Figure 1. Current density vs. electrode potential curves relating to Hf anodic film grown potentiodynamically in a) 0.1 M ABE and b) 0.1 M NaOH.

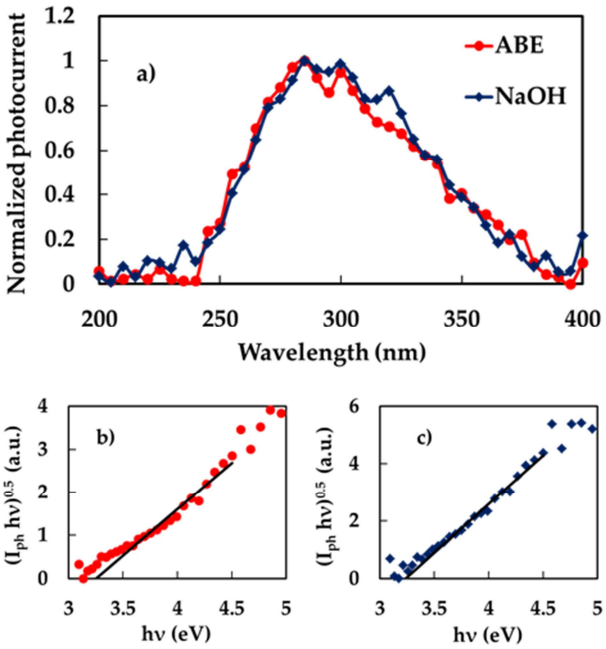

Figure 2. Anodic photocurrent spectra a) relating to anodic films grown on Hf in ABE and NaOH, recorded by polarizing the electrodes at 3 V vs. Ag/AgCl. Band gap estimate by assuming indirect optical transitions relating to the same anodic film grown in b) ABE and c) NaOH.

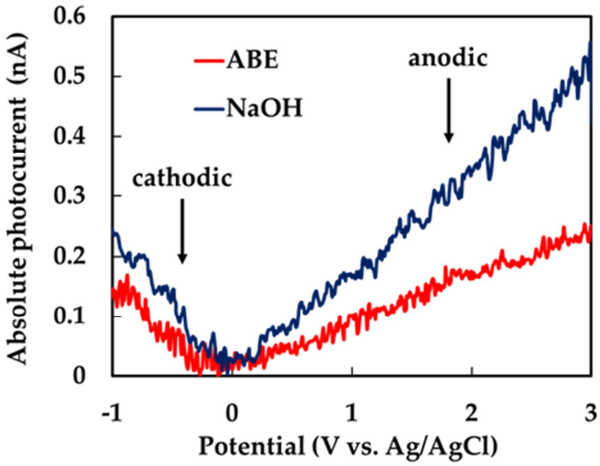

Figure 3. Absolute photocurrent vs. electrode potential curves relating to the 5 V anodic oxides grown in ABE and NaOH, recorded at constant irradiating photon wavelength (λ = 280 nm) in 0.1 M ABE by decreasing electrode potential at 10 mV s^{-1}.

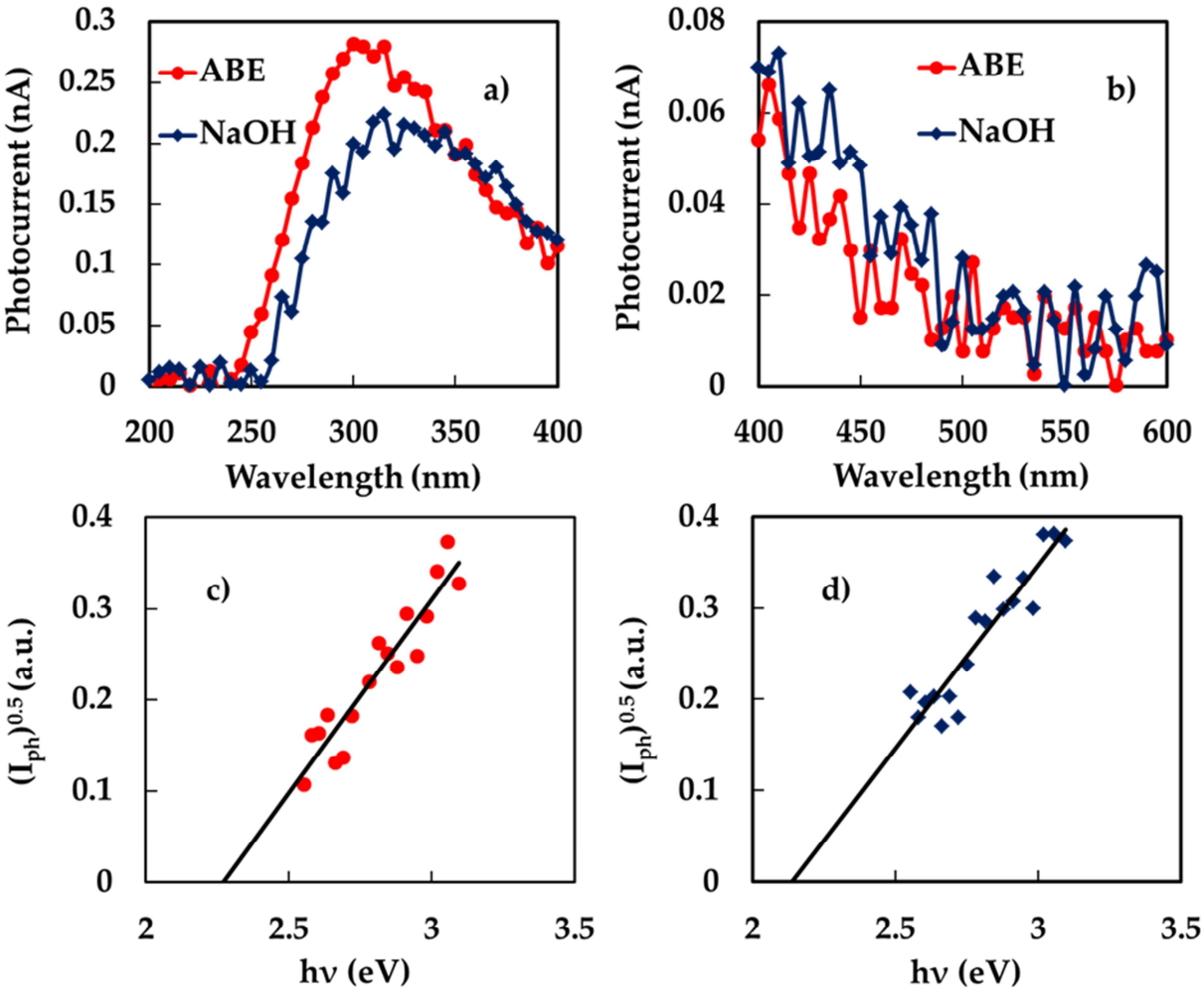

Figure 4. a) Cathodic photocurrent spectra relating to the oxides grown on Hf in ABE and NaOH recorded at - 1 V vs. Ag/AgCl as electrode potential. b) Long wavelength region of the photocurrent spectra, recorded by using a UV filter. Fowler plots relating to the oxides grown in c) ABE and d) NaOH.

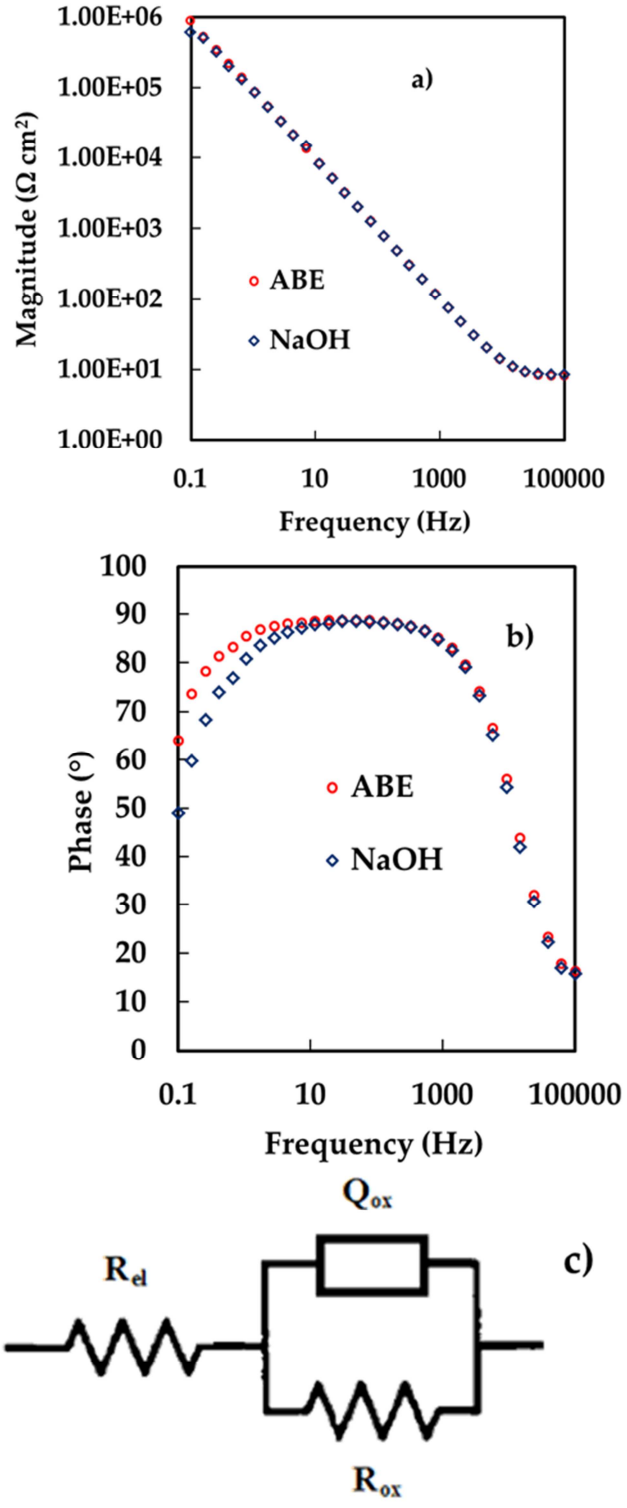

Figure 5. EIS spectra relating to Hf anodic films grown in ABE and NaOH electrolytes, recorded by polarizing the electrode at 3 V vs. Ag/AgCl in 0.25 M Na_2HPO_4. a) Magnitude, b) phase angle, c) electrical equivalent circuit employed to model the metal/oxide/electrolyte interfaces.

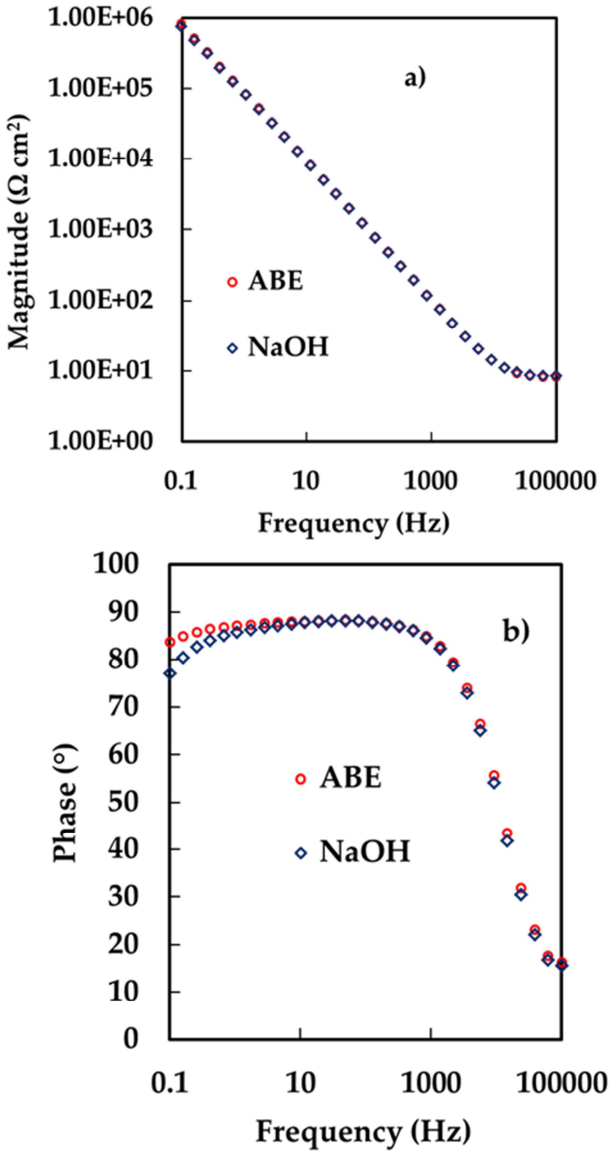

Figure 6. EIS spectra relating to Hf anodic films grown in ABE and NaOH electrolytes, recorded by polarizing the electrode at -1 V vs. Ag/AgCl in 0.25 M Na_2HPO_4. a) Magnitude and b) phase angle.

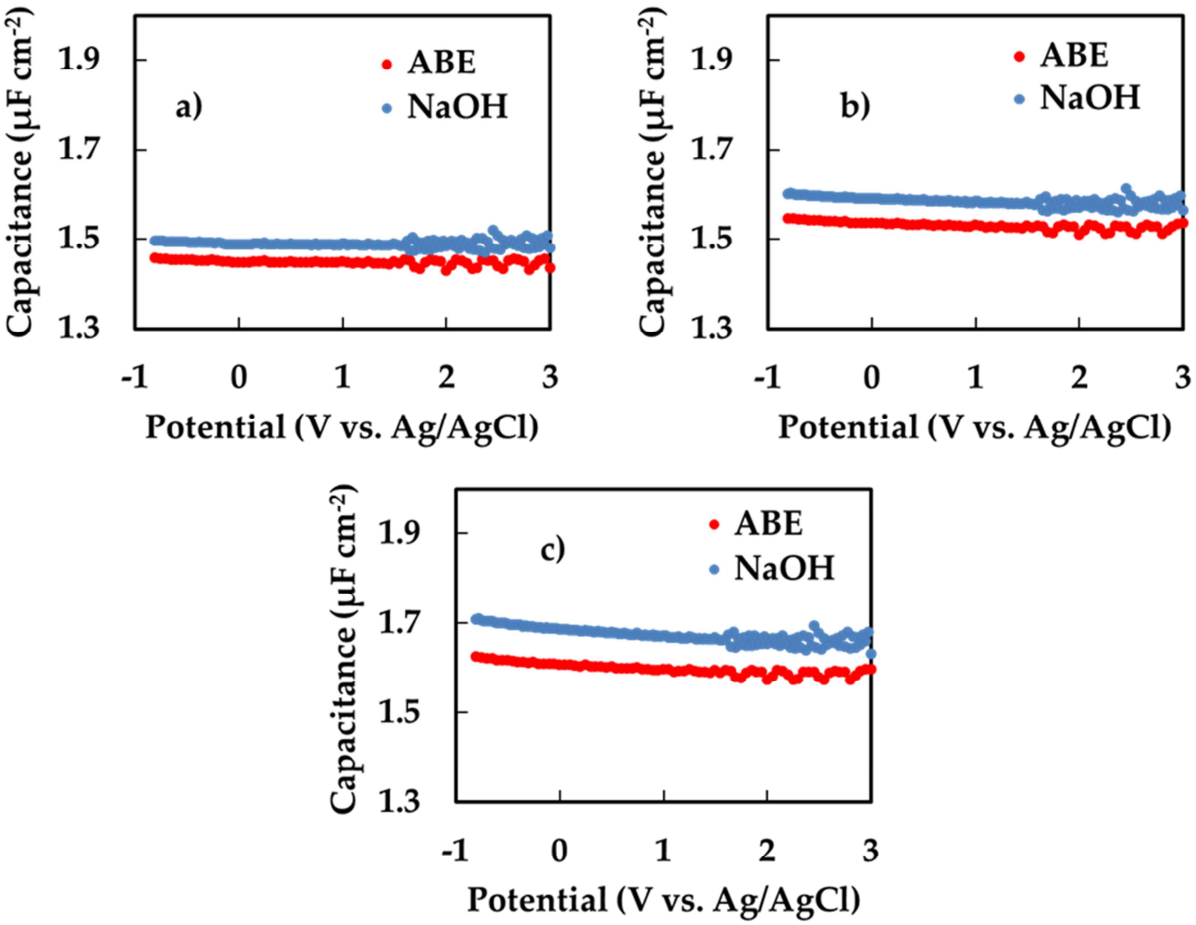

Figure 7. Measured series capacitance relating to 5 V Hf oxides grown in 0.1 M ABE and 0.1 M NaOH. A.c. signal frequencies: a) 10 kHz, b) 1 kHz and c) 100 Hz.

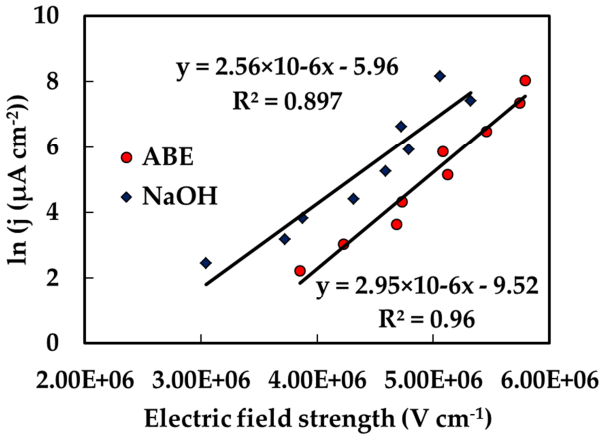

Figure 8. Tafel plot relating to Hf anodizing processes in 0.1 M ABE and 0.1 M NaOH.

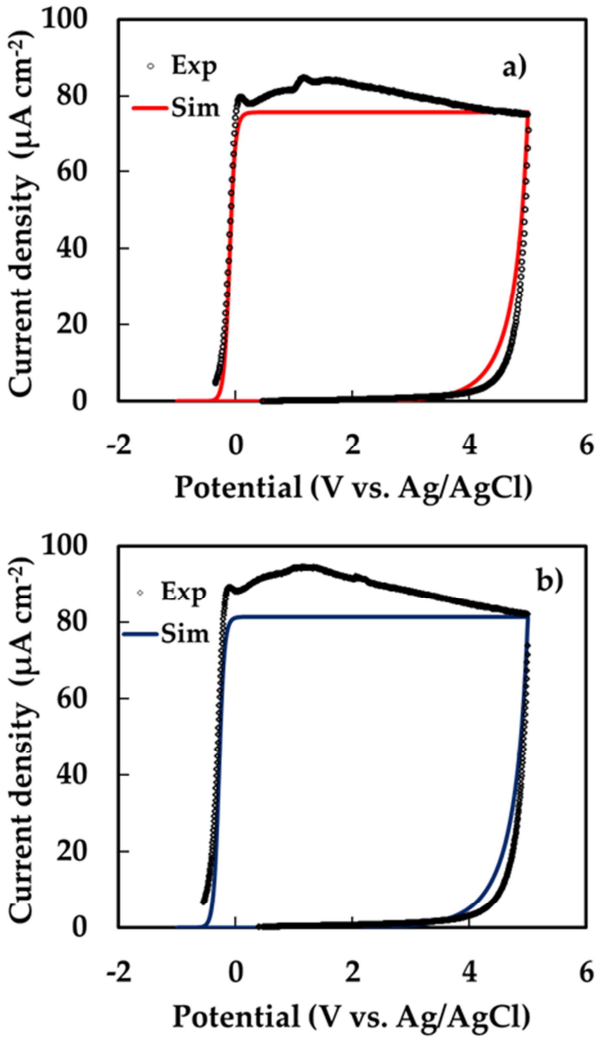

Figure 9. Experimental (symbols) and simulated (according to eq 6, continuous lines) current density vs. electrode potential curves relating to Hf anodic films growth in a) 0.1 M ABE and in b) 0.1 M NaOH. Growth scan rate: 20 mV s^{-1}.

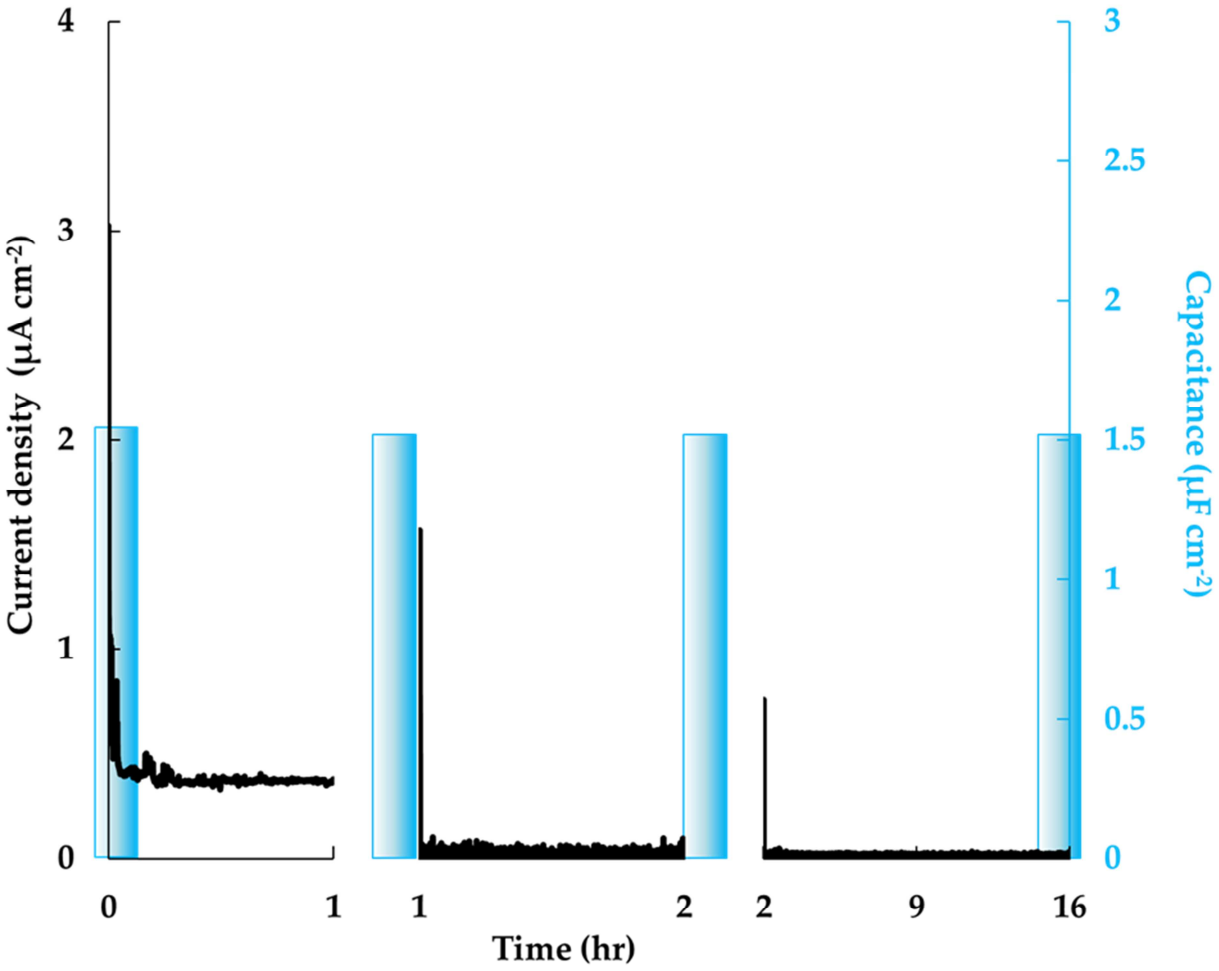

Figure 10. Capacitance (blue bars) and current density measurements vs. time during potentiostatic polarization at U_E = 3 V (Ag/AgCl) relating to Hf anodic oxide grown in 0.1 M NaOH at 20 mV s^{-1}.

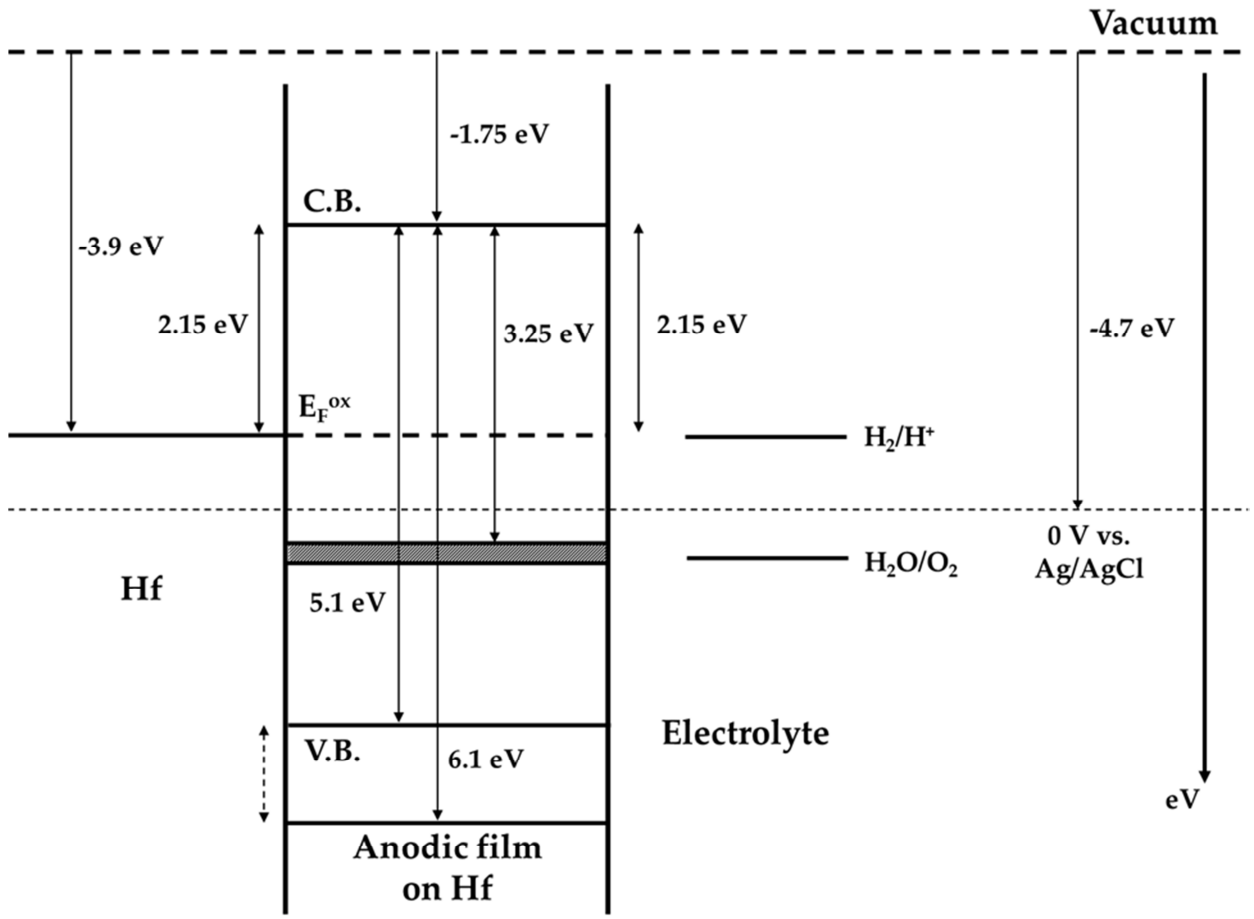

Figure 11. Approximate sketch of the energetic levels of metal/oxide/electrolyte interface for anodic films grown on Hf. Dotted arrow: energy interval in which valence band edge can be placed according to the literature.